Polymer 182 (2019) 121845

Contents lists available at ScienceDirect

Polymer

journal homepage: http://www.elsevier.com/locate/polymer

# 3D printing of polylactic-co-glycolic acid fiber scaffolds using an antisolvent phase separation process

Anton Vladimirovich Mironov *, Olga Anatolevna Mironova, Maria Aleksandrovna Syachina, Vladimir Karpovich Popov

*Institute of Photonic Technologies, Federal Scientific Research Center "Crystallography and Photonics", Russian Academy of Sciences, 108840, Moscow, Pionerskaya str. 2, Russian Federation*

ARTICLE INFO

*Keywords:*
Polymer scaffolds
Polylactic-co-glycolic acid (PLGA)
Tetraglycol (TG)
Antisolvent solidification
Phase separation
3D printing

ABSTRACT

We present the results of experimental studies into the computer-controlled fabrication of polylactic-co-glycolic acid (PLGA) scaffolds under conditions of diffusion and antisolvent phase separation of PLGA/tetraglycol (TG) solutions in aqueous media. The effect of the initial concentrations of the polymer solutions and the 3D printing process parameters on the type of the fiber structures formed was studied. The resultant scaffolds were found to be produced in the form of either fractal-like or spongy polymeric microstructures. The specific type of the structures formed was shown to depend on the intensity of the diffusion processes in the ternary system PLGA–TG–antisolvent. This approach can be used for highly efficient 3D printing of both microporous and hollow fiber biocompatible scaffolds of various architectonics.

## 1. Introduction

Tissue engineering today is one of the most advanced approaches to the solution of the pressing problems of regenerative medicine whereby the restoration of damaged or lost tissues is carried out using specially fabricated hybrid or bioartificial constructs [1–4]. In the general case, such tissue-engineering constructs (TEC) are combinations of certain types of live cells and artificial (generally bioresorbable) scaffolds that initially perform the functions of the natural intercellular matrix [5–7].

Such functions primarily include provision for adhesion of cells to the surface of the scaffold and also for their directional differentiation and efficient proliferation [8–11]. The material and structure of a given scaffold should be selected with due regard for the physicochemical, mechanical, and morphological properties of the native tissues at the site of its implantation. The scaffold should also feature the desired predictable character of biodegradation yielding nontoxic substances easy to remove from the organism [12–14].

In many cases the above-mentioned requirements can be met by polymer porous structures with a network of interconnected channels, which provide comfortable conditions for the growth of cells, delivery of nutrients to them, and removal of the metabolic wastes of their vital activity [15–23]. The porosity characteristics of such structures play a fairly important role, determining the processes of migration and ingrowth of cells deep into the scaffold, thus facilitating the formation of a new extracellular matrix [24,25].

Biocompatible polymers from the homological series of aliphatic polyesters (polylactic acid, polylactic-co-glycolic acid, poly(ε-caprolactone)s and their copolymers) are among the best-studied synthetic materials of suitable physicochemical and mechanical properties for the fabrication of TEC's capable of controlled biodegradation when in contact with living tissues, which have long been approved for use in clinical practice and extensively employed in biomedical investigations [26–32]. To make particular items of these polymers, use is, as a rule, made of the classical approaches to the processing of their melts or solutions [33–38]. Classed with the material disadvantages of these methods should be the need to use either elevated temperatures (100 °C and over) or toxic organic solvents. All these factors make it difficult to produce biomedical items containing thermolabile components (for example, growth factors or medicinal preparations), making at the same time for uncontrolled variation of the molecular-mass distribution of the parent polymer, and also force one to employ rather costly procedures to remove traces of toxic solvents from these items [39,40].

The above-described shortcomings can be avoided by using alternative solvents or plasticizers, such as dimethyl sulfoxide (DMSO),

* Corresponding author.
*E-mail addresses:* scftlab@gmail.com (A.V. Mironov), mironova.o.a@yandex.ru (O.A. Mironova), mariya.sya4ina@yandex.ru (M.A. Syachina), vladikarpopov@gmail.com (V.K. Popov).

https://doi.org/10.1016/j.polymer.2019.121845
Received 5 July 2019; Received in revised form 25 September 2019; Accepted 27 September 2019
Available online 27 September 2019
0032-3861/

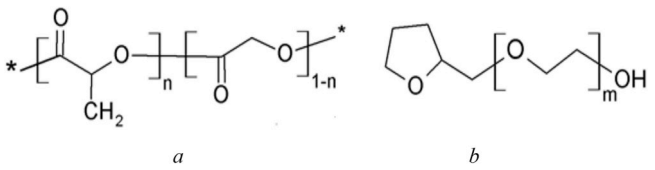

*a* *b*

**Fig. 1.** Structural formulas of (*a*) PLGA and (*b*) TG.

tetraglycol (TG) or supercritical carbon dioxide (sc-$CO_2$) [19,41–44], to process aliphatic polyesters.

Sc–$CO_2$–based technologies possess a high potential for aliphatic polyesters treatment. However, despite of their attractive advantages (environmental friendliness, high purity, single-stage processing, etc.), this methodology cannot be easily applied to reproducible and precise-controlled free form microstructure fabrication for custom-design biomedical devices. Mainly because of the stochastic nature of the processes of polymer internal structure formation during the expansion of sc-$CO_2$ plasticized material with its subsequent solidification.

DMSO and TG substances are capable of dissolving a variety of polymeric materials having highly limited solubility in water. By comparison with the chlororganic solvents traditionally used for polyesters, both DMSO and TG are less toxic and have a good thermodynamic compatibility with water, by virtue of which they can practically completely be extracted (removed) from a polymeric solution in any water-containing medium (for example, a culture fluid or intercellular lymph). Specifically this property is used to make medicinal preparations for parenteral injections [45,46]. The polymeric scaffold formed as a result of such a phase separation process can assume a fairly evolved microstructure (a porous one included) [25,47,48]; and this, as noted earlier, is one of the key requirements for the fabrication of TEC's [24,49,50]. At the same time, with all other things being equal, DMSO can manifest distinct cytotoxic effect for blood, vascular and skin different types of the living sell [51–53]. According to the literature it is caused by DMSO ability to penetrate through the cell membranes and transporting solutes into the cytoplasm. Thus, the use of DMSO significantly increases safety requirements for the composition of the scaffold and the implantation site. For this reason, we consider TG a more preferable candidate for the making of such implantable constructs.

We have earlier proposed, developed and implemented a process of antisolvent 3D printing of PLGA scaffolds with a radially oriented microstructure and with a system of interpenetrating pores for tissue engineering constructs (TEC) [54]. The results of our *in vitro* analysis of cytotoxicity and matrix properties of these 3D printed samples high potential of this for fabrication of bioresorbable scaffolds with computer-controlled architectonics for TECs. However, this work did not comprise the systematic and detail study of PLGA scaffold structural formation processes.

The present study is a logical outgrowth of the above-mentioned investigations. It is centered on detailed studies of the diffusion, phase separation, and structure formation processes occurring in PLGA solutions in TG on their contact with water-containing media. We believe that the described results could be useful for bioresorbable scaffolds fabrication with a free form reproducible architectonics and gives a way to control its microporous structures which are crucially important issues for TECs.

## 2. Materials and methods

### 2.1. Materials

The material used for the making of individual fibers and scaffolds was the commercially available polylactic-co-glycolic acid (PLGA) PURASORB PDLG7507 (Corbion Purac, the Netherlands) with a lactic-to-glycolic acid monomer ratio of 75:25 and a characteristic viscosity of 0.7 Pa s (Fig. 1*a*).

The solvent used for PLGA was tetrahydrofurfuryl polyethylene glycol (tetraglycol, TG) (CAS Number: 31692-85-0; Sigma-Aldrich, USA) with $M_n = 200$ whose structural formula is presented in Fig. 1*b*. Distilled water was used as a model antisolvent.

Used in the experiment were PLGA solutions in TG with concentrations of $C = 5$, 10, 15, 20, and 25 mass%. To obtain the solutions to be studied, from 0.15 to 0.78 g parent polymer was dissolved in 2 g TG. The solutions were intensively stirred with a magnetic mixer for 24 h in a hermetically sealed polypropylene container at a temperature of 40 °C.

### 2.2. Method of making individual fibers and scaffolds

#### 2.2.1. Experimental setup

The polymer fiber formation experiments were performed using the laboratory 3D printer (Fig. 2*a*) designed by us previously [55].

The fibers were formed by means of 8-mm long stainless steel hollow injection needles with an inner diameter of 200, 400, 500, 600, 750, 900, 1000, and 1300 μm (Fig. 2*a, b*). The 3D scaffold printing experiments used 8-mm long needles with an inner diameter of 200 μm (for solutions with a PLGA concentration from 5 to 15 mass%) and 400 μm (for solutions with a PLGA concentration of 20 and 25 mass%).

The working vessels for the 3D printing process were 120-mm-dia. Polystyrene Petri dishes filled with 120 ml distilled water at a temperature of 10, 25, or 40 °C. Immediately before the experiment, the dozer of the 3D printer containing a PLGA solution in TG was subjected to thermostating for 1 h at a temperature of 10, 25, or 40 °C.

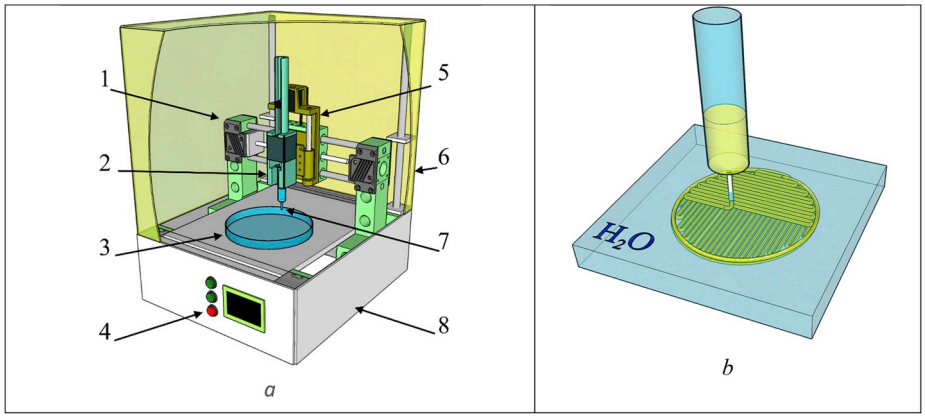


**Fig. 2.** Experimental setup for 3D printing with liquid compositions (a) and schematic illustration of the 3D printing process and the structure of a PLGA scaffold (b). 1 – *x*-axis motorized guide; 2 – dozer; 3 – vessel for printing; 4 – control panel; 5 – *z*-axis motorized guide; 6 – protective cover; 7 - dozer nozzle; 8 – printer casing.

#### 2.2.2. Fiber formation

To obtain experimental polymer fiber samples, a given PLGA solution in TG having the desired concentration and temperature was injected by the printer's dozer into a Petri dish filled with distilled water. Depending on the viscosity of the solution and the dozer nozzle diameter, the solution flow rate ranged from 0.015 to 14 μl/s. To finish the fiber solidification process, the samples obtained were immersed in containers with excess distilled water that were then placed for 24 h in a thermostat at a temperature of 37.8 °C. Thereafter the fibers were washed with 95-% ethyl alcohol and air dried at room temperature for 24 h.

#### 2.2.3. Printing of 3D structures

The digital models used in the process were layer-by-layer models of latticed discs 5 and 10 mm in diameter. The PLGA solution in TG of the desired concentration and temperature was injected by the printer's dozer into a Petri dish filled with distilled water, with the flow trajectory and rate being specified by the software of the 3D printer (Fig. 2*b*). To make the sample adhere to the Petri dish, the initial clearance between the tip of the dozer nozzle and the bottom of the Petri dish was set at 100 μm. Each subsequent layer was applied with a line pitch of 200 μm to the surface of the preceding one that had already solidified to some degree. The linear velocity of the dozer along the axes ranged between 0.25 and 8 mm/s for the flow rate of the given PLGA solution from 0.05 to 0.12 μl/s, depending on its concentration. The finished samples were washed twice with distilled water and then placed contained in excess distilled water in a thermostat at a temperature of 37.8 °C for 24 h. Thereafter the polymer scaffolds obtained were washed with 95-% ethyl alcohol and air dried at room temperature for 24 h.

### 2.3. Investigation methods

#### 2.3.1. Optical microscopy

The optical analysis of the scaffolds obtained was performed with a Model Bresser Advance ICQ stereoscopic microscope (Bresser, USA) equipped with a Levenhook C510 camera (Levenhook, USA) and ToupView software (TOUPTEK, South Korea). To this end, the samples were consecutively washed with distilled water and 95% ethanol, air dried at room temperature for 24 h, and then placed on microscope slides and investigated by reflected light.

#### 2.3.2. Scanning electron microscopy

The microstructure of the fibers obtained was investigated with a Model Phenom ProX scanning electron microscope (Phenom, the Netherlands). The accelerating voltage used to obtain the desired images was either 5 or 10 kV, with the magnification scale increasing from 50 to 1000. Prior to the studies, the samples were also sequentially washed with distilled water and 95% ethanol and then air dried at room temperature. The samples were fixed to the microscope stage with a conductive carbon tape, with no current-conducting (metallic) material being deposited on them.

#### 2.3.3. Rheology of the PLGA solutions in TG

The rheological characteristics of the parent PLGA solutions were studied with a Model μVisc viscometer (Rheosense, USA). During the course of measurements, the temperature of the solutions was maintained at 25 °C by means of a standard thermostat. The viscosity of the samples was automatically calculated from the pressure distribution in the channel of the VROC measuring chip (Rheosense, USA) with a 200-μm rectangular-slit channel (VROC 17HA201, viscosity range 10–2000 Pa s). For the PLGA solution with a concentration of $C = 5$ mass % use was additionally made of a measuring chip with a 50-μm slit channel (VROC 17HA051, viscosity range 0–100 Pa s). The rheological curves were constructed on the basis of the viscosity measurement results for the solutions under study obtained over the shear rate gradient range from 2 to 600 $s^{-1}$.

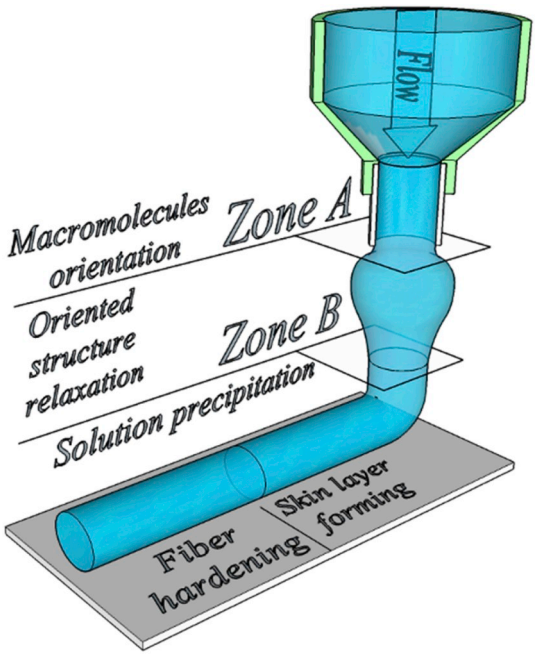


**Fig. 3.** Schematic illustration of the polymer solution-to-fiber transformation process.

## 3. Results and discussion

### 3.1. Fiber structure

The PLGA/TG solution stream-to-fiber transformation kinetics is governed by the sequence of processes taking place during the course of its injection into and solidification in an aqueous medium (Fig. 3).

Depending on the concentration and viscosity of the solution, the geometry and internal structure of the fiber produced varies continuously over its formation path. In the channel of the dozer nozzle the polymer macromolecules in the solution undergo oriented stretching along the flow axis owing to the radial velocity gradient (denoted by "zone A″ in Fig. 3). At the nozzle outlet there takes place the elastic recovery of the stream due to the Barrus effect (also known as die or extrudate swell), i.e., relaxation of the molecular structure of the solution (denoted by "zone B″ in Fig. 3) [56–58]. At the moment when the surface of the solution stream comes in contact with the antisolvent (water) there starts the phase separation of the solution and the resultant formation of a skin gel layer allowing the cross-diffusion of the antisolvent into and solvent (TG) out of the PLGA fiber to pass through.

The solutions studied were typical pseudoplastic fluids featuring a nonlinear relationship between the dynamic viscosity η and the shear rate gradient γ (Fig. 4*a*).

The flow curves, $\eta = f(\gamma)$, found were used to establish the concentration dependences of the shear rate at which the effective viscosity of the polymer solution dropped substantially because of its macromolecules getting oriented along the flow (curve *1* in Fig. 4*b*).

Using equation (1) below, we calculated the critical shear rate gradients for our experimental conditions, at which the polymer macromolecules in the solution stream get oriented (curve *2* in Fig. 4*b*):

$$\gamma_{max} = \frac{(1+3n)}{n} Q \Big/ \pi \cdot r^3 \quad (1)$$

where $Q$ is the volume flow rate, $mm^3/s$, $r$ is the nozzle radius, and $n$ is a parameter characterizing the deviation of the rheological properties of the given fluid from the Newtonian ones [59].

Comparison between the critical shear rates found and the calculated maximum shear rates made it possible to establish the fact that the flow

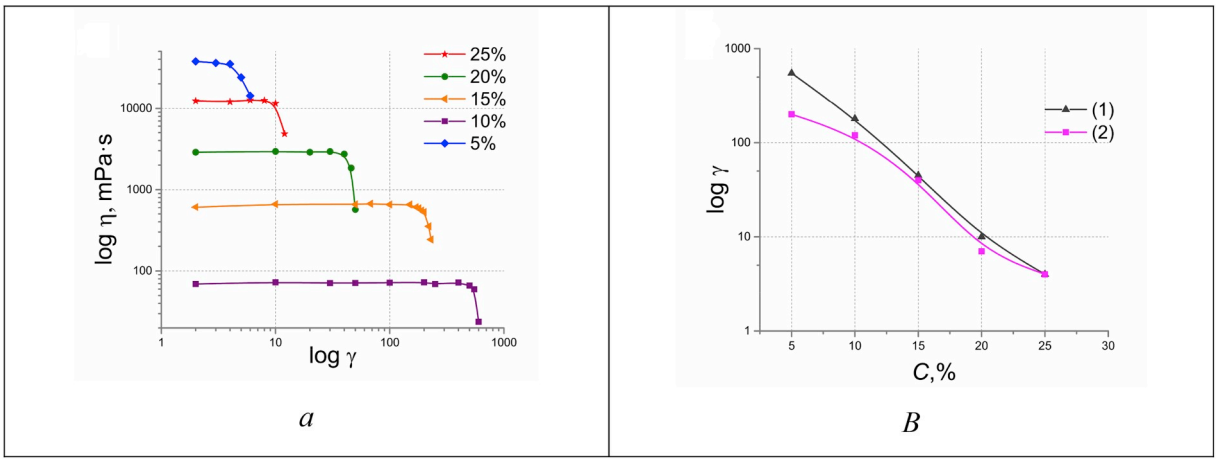


**Fig. 4.** (*a*) Flow curves of PLGA/TG solutions differing in concentration; (*b*) concentration dependences of the critical shear rate: curve *1* – experiment; curve *2* – theory.

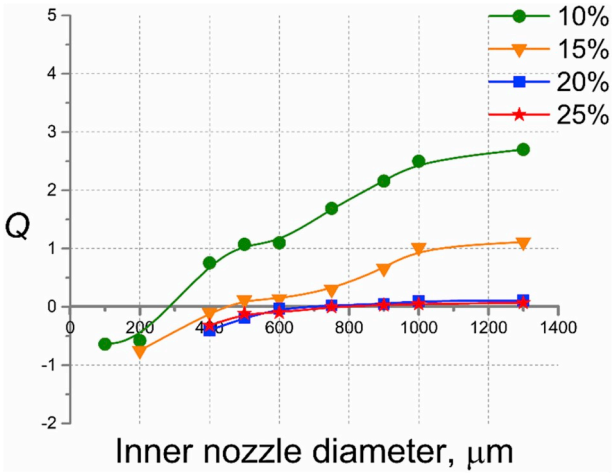


**Fig. 5.** Variation of the polymer solution stream geometry in the course of antisolvent deposition process. Q - the amount of fiber contraction or swelling calculated by equation (2).

rates used in our experiments did not exceed the threshold values necessary for the structure of the solution to get oriented. This allowed the contribution from the orientation/relaxation processes to the geometry and structure of the fiber being formed to be neglected. Considering the practically unlimited mutual solubility of TG and water, the surface tension forces at the polymer solution/antisolvent interface are initially very weak and have no substantial effect on the stability of the stream.

The variation of the cross-section of the fiber formed during the course of the antisolvent printing process correlates in a nonlinear fashion with the cross-section of the nozzle, the degree of this correlation being dependent on the viscosity of the source solution (Fig. 5). The amount of the fiber contraction or swelling ($Q$) was determined as the ratio between the specific volumes of the fiber, $V_f$, and the source solution stream, $V_n$:

$$Q = \frac{Vf - Vn}{Vn} \tag{2}$$

Considering that the shape of both the stream and fiber is very nearly cylindrical, $V = h{\cdot}\pi d2/4$, and the length of the fiber is constant, $h = \text{const}$, we have.

$$Q = \frac{h{\cdot}\pi{\cdot}d_f^2/4 - h{\cdot}\pi{\cdot}d_n^2/4}{h{\cdot}\pi{\cdot}d_n^2/4}$$

$$Q = \left(\frac{h{\cdot}\pi/4}{h^*{\cdot}\pi/4}\right)\left(\frac{d_f^2 - d_n^2}{d_n^2}\right) = \frac{d_f^2 - d_n^2}{d_n^2}$$

$$Q = \frac{d_f^2}{d_f^2} - 1 \tag{3}$$

The change in the geometry of the polymer solution stream in the course of formation of the fiber bears witness to the fact that the mass-exchange process involves a series of consecutive stages. In the initial, solvent diffusion, stage, the formation of the surface gel membrane is accompanied by an intensive extraction of TG and the correspondent reduction of the fiber cross-section. In the second, antisolvent diffusion, stage, the directed flow of water into the bulk of the fiber causes the latter to swell. Contraction is only typical of small-diameter streams from 200 to 500 μm in diameter, wherein phase separation comes to an end within a short period of time (1–2 s) at the solvent diffusion stage. For the streams of solutions whose fluidity remained for a few seconds (streams over 600 μm in diameter; 10 and 15 mass% in concentration), the somewhat later diffusion of the antisolvent inside the fiber results in a substantial enlargement of its volume. More viscous solutions (20 and 25 mass% in concentration) lose their fluidity within a relatively short

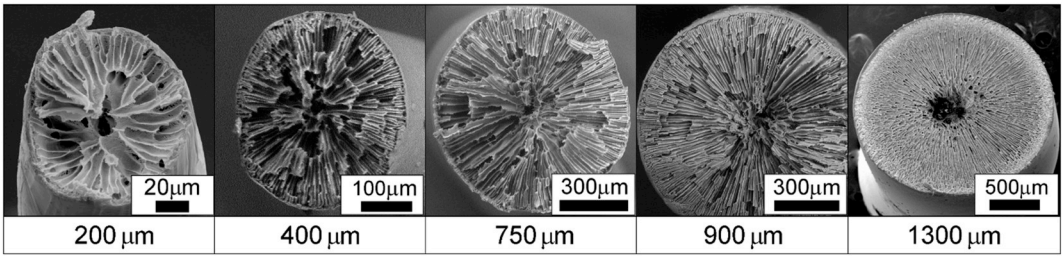


**Fig. 6.** SEM images of PLGA fibers internal structure depending on initial jet diameter of the solutions with a polymer concentration $C = 15$ mass%.

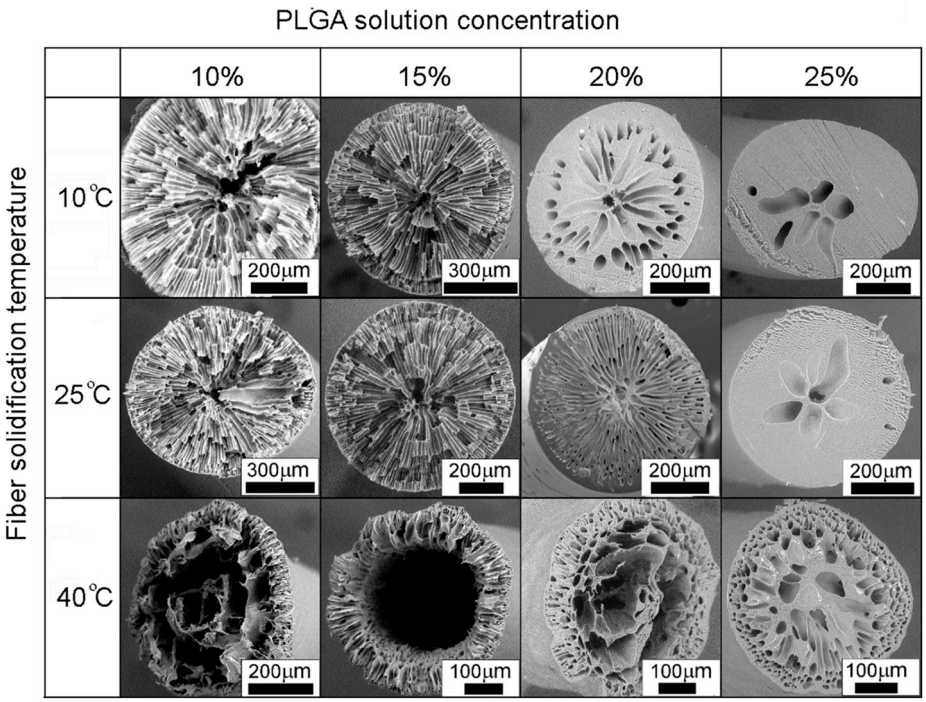


**Fig. 7.** SEM images of polymer fiber structures fabricated from the solutions with a different initial PLGA concentration at different solidification temperature.

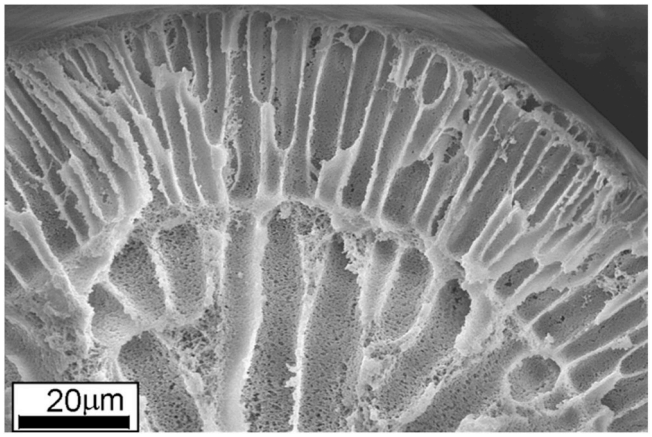


**Fig. 8.** SEM image of PLGA fiber cross-section with an internal interface fabricated from PLGA solutions with concentration $C = 10$ mass% at $T = 25\,^{\circ}C$.

period of time (on the order of 1 s) and practically do not swell, their contraction being largely due to syneresis taking place in the course of formation of the gel structure.

The microscopic analysis of sections of fibers obtained from PLGA solutions differing in concentration showed that their internal structure was determined by the viscosity and formation time of the gel fiber containing residual solvent. The solidification of a small-diameter stream led to the formation of a branched porous centrally symmetric structure that gradually became more ordered as the fiber diameter was increased (Fig. 6).

Because the concentration of the polymer phase grows higher at the solvent/antisolvent contact surface, the fiber formation started from the skin membrane and proceeded toward the center by the matrix mechanism. As a result, the fibers obtained featured a radial density gradient owing to the polymer concentration gradient in their parent solutions. In the case of PLGA solutions 10 and 15 mass% in concentration, as well as with streams of large diameter (i.e., in conditions of relatively low viscosity and minimal phase separation rate), the intensive cross solvent/antisolvent mass transfer resulted in the formation of fibers having a ring-shaped cross-section with a central hollow (Fig. 6 and 1300 μm).

The temperature- and concentration-dependent viscosity of PLGA solutions in TG has a substantial effect on the internal structure of the fibers formed. In the general case, for temperatures below 25 °C, the fibers showed a radially oriented microstructure associated with the development of intensive counter flows of the polymer solution and antisolvent during the solidification process of the former (Fig. 7). The sole exception was the fiber obtained from the most viscous PLGA solution (25 mass% in concentration) at low solidification temperatures (10 and 25 °C).

In some cases, the structure of the fiber exhibited a radial heterogeneity stemming from the periodicity of formation of oversaturation and phase-separation zones during the course of the cross solvent/antisolvent diffusion (Fig. 8).

As the temperature of the solution was raised to 40 °C, with its effective viscosity being reduced correspondingly, the fibers produced were observed to undergo an insignificant reduction in diameter and some loosening in structure, no matter what the concentration of their parent solutions. The relatively ordered internal structure of the fibers turned into a more chaotic one, a ring-shaped cross-section now being obtained for solutions from 10 to 20 mass% in concentration and with smaller diameters of the source streams (Figs. 7 and 40 °C).

**Table 1**
Parameters of 3D printing of PLGA scaffolds using a 200-μm-dia. Nozzle.

| Concentration, % | Nozzle diameter, μm | Solution flow rate, μl/s | Linear dozer velocity, mm/s | Characteristic |
|---|---|---|---|---|
| 5 | 200 | 0.16 | 5 | Stream disintegration |
| 10 | 200 | 0.1 | 3.5 | 3D structure |
| 15 | 200 | 0.03 | 1 | 3D structure |
| 20 | 400 | 0.04 | 0.3 | Individual fibers |
| 25 | 400 | 0.031 | 0.25 | Individual fibers |

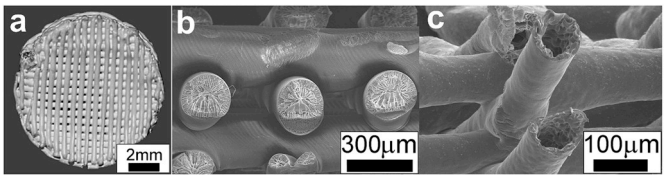


**Fig. 9.** (a) Appearance of scaffolds 3D printed from 15-mass% PLGA solutions in TG; (*b*) and (c) SEM images of the scaffold structures formed at 25 °C and 40 °C, respectively.

### 3.2. Structure of three-dimensional scaffolds

The rheological characteristics of the source PLGA solutions in TG exert a material effect on the process of formation of hard polymeric 3D structures from them. Because there are no surface tension forces in the aqueous medium and the cohesive strength of the solution stream is not very high, the solution flow rate and the 3D printing speed were selected so as to suit the rheology of the solution (Fig. 4*b*) and minimize axial loads on the fiber being formed. The linear velocities of the dozer along the axes and the volume flow rates of the PLGA solutions in TG are listed in Table 1.

We failed experimentally to obtain 3D scaffolds for the entire range of the PLGA solutions investigated. The viscosity of the 5-mass% PLGA solution was too low, and so the solution stream got disintegrated within a very short period of time (less than 1 s) irrespective of the experimental conditions. When printing fibers from 20- and 25-mass% solutions, we failed to obtain any coherent structures, for the promptly formed hard skin layer of the fibers prevented them from cohesion. Mechanically stable scaffolds were successfully formed from 10- and 15-mass% PLGA solutions in the temperature range from 25 to 40 °C using a 200-μm-dia. Nozzle (Fig. 9*a*), the 3D structures being formed by fibers whose final diameter came, because of contraction, to 140–150 μm.

The structure formation of the fibers making up a three-dimensional scaffold ran its course in the same way as the above-described process with model fibers. As the temperature of the PLGA solution grew higher, the reduction of is viscosity made the fibers formed uneven, with their mean diameter ranging between 80 and 100 μm, and increased the degree of their contraction. The porous structure of the fibers changed to a tubular one, which in the last analysis led to the impairment of the mechanical strength of the three-dimensional structures formed (Fig. 9*c*).

## 4. Conclusions

Our investigations of the diffusion, phase-separation, and structure formation processes taking place in PLGA solutions in TG on their contact with distilled water demonstrated that the rheological characteristics of the parent solutions exert a decisive effect on the morphological parameters of the bioresorbabable structures formed by the antisolvent 3D printing method developed by us. In the course of formation of the gel sheath on the fiber, a certain viscosity of the PLGA solution provides for the stability of its stream by preventing it from both wash-out and excessive contraction.

The conditions of formation of the internal structure of the fiber depend on the concentration and temperature of its source solution, i.e., the factors determining the viscosity of the solution and the solidification rate of the fiber. The internal structure of the fiber (the character and distribution of its pores) is practically wholly determined by the viscosity of the source solution and the kinetics of the radially directed diffusion processes in the ternary system PLGA–TG-antisolvent. The solidification of a small-diameter solution stream results in the formation of a fiber with a porous centrally symmetric internal structure whose characteristic size depends inversely on the fiber diameter. It was shown experimentally that the relationships found by us to govern the formation of the internal microstructure of PLGA fibers can be used to make scaffolds differing in architectonics of both microporous and hollow fibers around 100 μm in characteristic diameter for tissue engineering constructs by the antisolvent 3D printing method.

## Acknowledgements

This work was supported by the Ministry of Science and Higher Education of the Russian Federation within the State assignment FSRC « Crystallography and Photonics » RAS in part dealing with rheological studies and by the Russian Foundation for Basic Research (Project No. 16-29-11722) in all other parts of this work.

## Appendix A. Supplementary data

Supplementary data to this article can be found online at https://doi.org/10.1016/j.polymer.2019.121845.

## References

[1] D.W. Hutmacher, J.C.H. Goh, S.H. Teoh, An introduction to biodegradable materials for tissue engineering applications, Ann. Acad. Med. Singapore 30 (2) (2001) 183–191.
[2] B.E. Chaignaud, R. Langer, J.P. Vacanti, The history of tissue engineering using synthetic biodegradable polymer scaffolds and cells, Synth. Biodegrad. Polym. Scaffolds (2011), https://doi.org/10.1007/978-1-4612-4154-6_1.
[3] M. Martina, D.W. Hutmacher, Biodegradable polymers applied in tissue engineering research: a review, Polym. Int. (2007), https://doi.org/10.1002/pi.2108.
[4] G.P. Reece, C.W. Patrick, Tissue engineered construct design principles, Front. Tissue Eng. (2008), https://doi.org/10.1016/b978-008042689-1/50012-1.
[5] W.L. Murphy, R.G. Dennis, J.L. Kileny, D.J. Mooney, Salt fusion: an approach to improve pore interconnectivity within tissue engineering scaffolds, Tissue Eng. (2002), https://doi.org/10.1089/107632702753503045.
[6] H. Frommelt, Polymers for medical applications, Makromol. Chem. Macromol. Symp. (1987), https://doi.org/10.1002/masy.19870120114.
[7] S. Jockenhoevel, G. Zund, S.P. Hoerstrup, K. Chalabi, J.S. Sachweh, L. Demircan, B. J. Messmer, M. Turina, Fibrin gel - advantages of a new scaffold in cardiovascular tissue engineering, Eur. J. Cardiothorac. Surg. (2001), https://doi.org/10.1016/S1010-7940(01)00624-8.
[8] D.W. Hutmacher, S. Cool, Concepts of scaffold-based tissue engineering - the rationale to use solid free-form fabrication techniques, J. Cell Mol. Med. (2007), https://doi.org/10.1111/j.1582-4934.2007.00078.x.
[9] L. Bacakova, E. Filova, M. Parizek, T. Ruml, V. Svorcik, Modulation of cell adhesion, proliferation and differentiation on materials designed for body implants, Biotechnol. Adv. (2011), https://doi.org/10.1016/j.biotechadv.2011.06.004.
[10] L. Bacakova, V. Mares, V. Lisa, V. Svorcik, Molecular Mechanisms of Improved Adhesion and Growth of an Endothelial Cell Line Cultured on Polystyrene Implanted with Fluorine Ions, Biomaterials, 2000.
[11] H. Hatakeyama, A. Kikuchi, M. Yamato, T. Okano, Patterned Biofunctional Designs of Thermoresponsive Surfaces for Spatiotemporally Controlled Cell Adhesion, Growth, and Thermally Induced Detachment, Biomaterials, 2007, https://doi.org/10.1016/j.biomaterials.2007.04.019.
[12] J. Idaszek, E. Kijeńska, M. Łojkowski, W. Swieszkowski, How important are scaffolds and their surface properties in regenerative medicine, Appl. Surf. Sci. (2016), https://doi.org/10.1016/j.apsusc.2016.03.038.
[13] H.-I. Chang, Y. Wang, Cell responses to surface and architecture of tissue engineering scaffolds, in: Regen. Med. Tissue Eng. - Cells Biomater, 2012, https://doi.org/10.5772/21983.
[14] Y. Ito, Surface Micropatterning to Regulate Cell Functions, Biomaterials, 1999, https://doi.org/10.1016/S0142-9612(99)00162-3.
[15] A.G. Mikos, G. Sarakinos, M.D. Lyman, D.E. Ingber, J.P. Vacanti, R. Langer, Prevascularization of porous biodegradable polymers, Biotechnol. Bioeng. (1993), https://doi.org/10.1002/bit.260420606.
[16] S.V. Madihally, H.W.T. Matthew, Porous Chitosan Scaffolds for Tissue Engineering, Biomaterials, 1999, https://doi.org/10.1016/S0142-9612(99)00011-3.
[17] A. Rogina, L. Pribolšan, A. Hanžek, L. Gómez-Estrada, G. Gallego Ferrer, I. Marijanović, M. Ivanković, H. Ivanković, Macroporous poly(lactic acid) construct supporting the osteoinductive porous chitosan-based hydrogel for bone tissue engineering, Polymer 98 (2016) 172–181, https://doi.org/10.1016/j.polymer.2016.06.030.
[18] L. He, Y. Zhang, X. Zeng, D. Quan, S. Liao, Y. Zeng, J. Lu, S. Ramakrishna, Fabrication and characterization of poly(l-lactic acid) 3D nanofibrous scaffolds with controlled architecture by liquid-liquid phase separation from a ternary polymer-solvent system, Polymer 50 (2009) 4128–4138, https://doi.org/10.1016/j.polymer.2009.06.025.
[19] Y. Reinwald, R.K. Johal, A.M. Ghaemmaghami, F.R.A.J. Rose, S.M. Howdle, K. M. Shakesheff, Interconnectivity and permeability of supercritical fluid-foamed scaffolds and the effect of their structural properties on cell distribution, Polymer 55 (2014) 435–444, https://doi.org/10.1016/j.polymer.2013.09.041.

[20] V.T. Bui, V.D. Dao, H.S. Choi, Transferable thin films with sponge-like porous structure via improved phase separation, Polymer 101 (2016) 184–191, https://doi.org/10.1016/j.polymer.2016.08.063.

[21] Q. Xing, X. Dong, R. Li, H. Yang, C.C. Han, D. Wang, Morphology and performance control of PLLA-based porous membranes by phase separation, Polymer 54 (2013) 5965–5973, https://doi.org/10.1016/j.polymer.2013.08.007.

[22] F.J. Hua, T.G. Park, D.S. Lee, A facile preparation of highly interconnected macroporous poly(D,L-lactic acid-co-glycolic acid) (PLGA) scaffolds by liquid-liquid phase separation of a PLGA-dioxane-water ternary system, Polymer (2003), https://doi.org/10.1016/S0032-3861(03)00025-9.

[23] J. Reignier, M.A. Huneault, Preparation of interconnected poly(ε{lunate}-caprolactone) porous scaffolds by a combination of polymer and salt particulate leaching, Polymer 47 (2006) 4703–4717, https://doi.org/10.1016/j.polymer.2006.04.029.

[24] M.D. Krebs, K.A. Sutter, A.S.P. Lin, R.E. Guldberg, E. Alsberg, Injectable poly (lactic-co-glycolic) acid scaffolds with in situ pore formation for tissue engineering, Acta Biomater. (2009), https://doi.org/10.1016/j.actbio.2009.04.035.

[25] K. Doi, T. Matsuda, Significance of porosity and compliance of microporous, polyurethane- based microarterial vessel on neoarterial wall regeneration, J. Biomed. Mater. Res. (1997), https://doi.org/10.1002/(SICI)1097-4636(19971215)37:4<573::AID-JBM17>3.0.CO;2-9.

[26] M. Vert, S.M. Li, G. Spenlehauer, P. Guerin, Bioresorbability and biocompatibility of aliphatic polyesters, J. Mater. Sci. Mater. Med. (1992), https://doi.org/10.1007/BF00701240.

[27] L. Wang, S. Venkatraman, L.H. Gan, L. Kleiner, Structure formation in injectable poly(lactide-co-glycolide) depots. II. Nature of the gel, J. Biomed. Mater. Res. B Appl. Biomater. (2005), https://doi.org/10.1002/jbm.b.30147.

[28] J. Hu, X. Liu, P.X. Ma, Induction of Osteoblast Differentiation Phenotype on Poly(l-Lactic Acid) Nanofibrous Matrix, Biomaterials, 2008, https://doi.org/10.1016/j.biomaterials.2008.06.015.

[29] J. Idaszek, A. Bruinink, W.-więszkowski, Delayed degradation of poly(lactide-co-glycolide) accelerates hydrolysis of poly(ε-caprolactone) in ternary composite scaffolds, Polym. Degrad. Stab. (2016), https://doi.org/10.1016/j.polymdegradstab.2015.12.020.

[30] X. Zhao, L. Liu, J. Wang, Y. Xu, W. Zhang, G. Khang, X. Wang, In vitro vascularization of a combined system based on a 3D printing technique, J. Tissue Eng. Regenerat. Med. (2016), https://doi.org/10.1002/term.1863.

[31] D. Ding, Q. Zhu, Recent advances of PLGA micro/nanoparticles for the delivery of biomacromolecular therapeutics, Mater. Sci. Eng. C (2018), https://doi.org/10.1016/j.msec.2017.12.036.

[32] G. Vozzi, C.J. Flaim, F. Bianchi, A. Ahluwalia, S. Bhatia, Microfabricated PLGA scaffolds: a comparative study for application to tissue engineering, Mater. Sci. Eng. C 20 (2002) 43–47, https://doi.org/10.1016/S0928-4931(02)00011-5.

[33] E.C. Bernhardt, Processing of Thermoplastic Materials, 1974.

[34] M.G. Devi, M. Amutheesan, R. Govindhan, B. Karthikeyan, A review of three-dimensional printing for biomedical and tissue engineering applications, Open Biotechnol. J. (2018), https://doi.org/10.2174/1874070701812010241.

[35] S.M. Giannitelli, D. Accoto, M. Trombetta, A. Rainer, Current trends in the design of scaffolds for computer-aided tissue engineering, Acta Biomater. (2014), https://doi.org/10.1016/j.actbio.2013.10.024.

[36] D.J. Yoo, Advanced porous scaffold design using multi-void triply periodic minimal surface models with high surface area to volume ratios, Int. J. Precis. Eng. Manuf. (2014), https://doi.org/10.1007/s12541-014-0516-5.

[37] M. Vaezi, H. Seitz, S. Yang, A review on 3D micro-additive manufacturing technologies, Int. J. Adv. Manuf. Technol. (2013), https://doi.org/10.1007/s00170-012-4605-2.

[38] D.W. Abueidda, M. Bakir, R.K. Abu Al-Rub, J.S. Bergström, N.A. Sobh, I. Jasiuk, Mechanical properties of 3D printed polymeric cellular materials with triply periodic minimal surface architectures, Mater. Des. (2017), https://doi.org/10.1016/j.matdes.2017.03.018.

[39] A.S. Goldstein, G. Zhu, G.E. Morris, R.K. Meszlenyi, A.G. Mikos, Effect of osteoblastic culture conditions on the structure of poly(DL-lactic-co-glycolic acid) foam scaffolds, Tissue Eng. 5 (1999) 421–434.

[40] D.J. Mooney, D.F. Baldwin, N.P. Suh, J.P. Vacanti, R. Langer, Novel approach to fabricate porous sponges of poly(D,L-lactic-co-glycolic acid) without the use of organic solvents, Biomaterials (1996), https://doi.org/10.1016/0142-9612(96)87284-X.

[41] E. Huang, X. Liao, Y. He, B. He, Q. Yang, G. Li, A novel route to the generation of porous scaffold based on the phase morphology control of co-continuous poly (ε-caprolactone)/polylactide blend in supercritical CO2, Polymer 118 (2017) 163–172, https://doi.org/10.1016/j.polymer.2017.04.065.

[42] I. Tsivintzelis, S.I. Marras, I. Zuburtikudis, C. Panayiotou, Porous poly(l-lactic acid) nanocomposite scaffolds prepared by phase inversion using supercritical CO2 as antisolvent, Polymer 48 (2007) 6311–6318, https://doi.org/10.1016/j.polymer.2007.08.021.

[43] I. Tsivintzelis, A.G. Angelopoulou, C. Panayiotou, Foaming of polymers with supercritical CO2: an experimental and theoretical study, Polymer 48 (2007) 5928–5939, https://doi.org/10.1016/j.polymer.2007.08.004.

[44] C. Tsioptsias, M.K. Paraskevopoulos, D. Christofilos, P. Andrieux, C. Panayiotou, Polymeric hydrogels and supercritical fluids: the mechanism of hydrogel foaming, Polymer 52 (2011) 2819–2826, https://doi.org/10.1016/j.polymer.2011.04.043.

[45] G. Bonacucina, G.F. Palmieri, Acrylic polymers as thickening agents for tetraglycol cosolvent, J. Pharm. Sci. (2006), https://doi.org/10.1002/jps.20567.

[46] H.W. Nielsen, E. Bechgaard, B. Twile, E. Didriksen, H. Sørensen, Intranasal administration of different liquid formulations of bumetanide to rabbits, Int. J. Pharm. (2000), https://doi.org/10.1016/S0378-5173(00)00461-0.

[47] S. Wu, X. Liu, K.W.K. Yeung, C. Liu, X. Yang, Biomimetic porous scaffolds for bone tissue engineering, Mater. Sci. Eng. R Rep. (2014), https://doi.org/10.1016/j.mser.2014.04.001.

[48] A. Moriya, T. Maruyama, Y. Ohmukai, T. Sotani, H. Matsuyama, Preparation of poly(lactic acid) hollow fiber membranes via phase separation methods, J. Membr. Sci. (2009), https://doi.org/10.1016/j.memsci.2009.07.005.

[49] S. Li, I. Molina, M. Bueno Martinez, M. Vert, Hydrolytic and enzymatic degradations of physically crosslinked hydrogels prepared from PLA/PEO/PLA triblock copolymers, J. Mater. Sci. Mater. Med. (2002), https://doi.org/10.1023/A:1013651022431.

[50] J.H. Byun, H.A.R. Lee, T.H. Kim, J.H. Lee, S.H. Oh, Effect of porous polycaprolactone beads on boneregeneration: preliminary in vitro and in vivo studies, Biomater. Res. (2014), https://doi.org/10.1186/2055-7124-18-18.

[51] X. Yi, M. Liu, Q. Luo, H. Zhuo, H. Cao, J. Wang, Y. Han, Toxic effects of dimethyl sulfoxide on red blood cells, platelets, and vascular endothelial cells in vitro, FEBS Open Bio (2017), https://doi.org/10.1002/2211-5463.12193.

[52] M. Singh, K. Mckenzie, X. Ma, Effect of dimethyl sulfoxide on in vitro proliferation of skin fibroblast cells, J. Biotech Res. 8 (2017) 78–82.

[53] J. Hebling, L. Bianchi, F.G. Basso, D.L. Scheffel, D.G. Soares, M.R.O. Carrilho, D. H. Pashley, L. Tjäderhane, C.A. De Souza Costa, Cytotoxicity of dimethyl sulfoxide (DMSO) in direct contact with odontoblast-like cells, Dent. Mater. (2015), https://doi.org/10.1016/j.dental.2015.01.007.

[54] A.V. Mironov, A.M. Grigoryev, L.I. Krotova, N.N. Skaletsky, V.K. Popov, V. I. Sevastianov, 3D printing of PLGA scaffolds for tissue engineering, J. Biomed. Mater. Res. A (2017), https://doi.org/10.1002/jbm.a.35871.

[55] A.V. Mironov, A.O. Mariyanac, O.A. Mironova, V.K. Popov, Laboratory 3D printing system, Int. J. Eng. Technol. (2018), https://doi.org/10.14419/ijet.v7i2.23.11886.

[56] D.W. Van Krevelen, K. Te Nijenhuis, Chapter 15 Rheological Properties of Polymer Melts, 2009, https://doi.org/10.1016/B978-0-08-054819-7.00015-7.

[57] Y. Tomita, T. Shimbo, Y. Ishibashi, Experimental studies of viscoelastic fluid flow, J. Nonnewton. Fluid Mech. (1979), https://doi.org/10.1016/0377-0257(79)85032-6.

[58] S.P. Sajjadi, Impact of die materials on the effect of new polymer processing aids for sharkskin properties, J. Mater. Sci. Chem. Eng. (2016), https://doi.org/10.4236/msce.2016.49002.

[59] J.S. Villiam, Introduction to Fluid Mechanics, fourth ed., 2012.